Diffusion of a Rouse chain in porous media: A mode-coupling-theory study

Huai Ding,[1] Huijun Jiang,[1] Nanrong Zhao,[2,*] and Zhonghuai Hou[1,†]

[1]*Department of Chemical Physics & Hefei National Laboratory for Physical Sciences at Microscales, University of Science and Technology of China, Hefei, Anhui 230026, China*

[2]*College of Chemistry, Sichuan University, Chengdu 610064, China*

(Received 24 July 2016; revised manuscript received 25 November 2016; published 12 January 2017)

We use a kinetic mode-coupling theory (MCT) combining with generalized Langevin equation (GLE) to study the diffusion and conformational dynamics of a bead-spring Rouse chain (RC) dissolved in porous media. The media contains fluid particles and immobile matrix ones wherein the latter leads to the lack of translational invariance. The friction kernel $\zeta(t)$ used in the GLE can be obtained directly by adopting a simple density-functional approach in which the density correlators calculated by MCT equations of porous media serve as inputs. Due to cage effects generated by surrounding particles, $\zeta(t)$ shows a very long tail memory in the high volume fraction of fluid and matrix. It is found that the long-time center-of-mass diffusion constant D_{CM} of the RC decreases with the increment of volume fraction, influencing more strongly by the matrix particles than by the fluid ones. The auto-correlation function (ACF) of the end-to-end distance fluctuation can also be calculated theoretically based on GLE. Of particular interest is that the power-law region of ACF has a nearly fixed length in logarithmic scale when it shifts to longer time range, with increasing the volume fraction of media particles. Moreover, the effect of lack of translational invariance has been investigated by comparing the results between fluid-matrix and pure fluid cases under identical total volume fraction.

DOI: 10.1103/PhysRevE.95.012121

I. INTRODUCTION

Diffusion properties of macromolecules in crowding environment have gained extensive study due to the broad importance in diverse fields ranging from material science to biophysics and medical science [1–13]. Especially in cell systems, the gradually decreasing space resulted from existence of crowders such as skeletal proteins [14] and membranes [15] influence remarkably the transport mechanisms and other biochemical processes. For example, C. Echeverria *et al.* studied the enzymatic dynamics of protein in solution with hard spherical obstacles [16], finding that the enzymatic cycle time and characteristic time of internal conformational motion are distinctly different from these values in simple systems. They also investigated the crowded effect caused by mobile macromolecules, showing that enzyme reaction kinetics can be considerably modified by those macromolecules, which also leads to subdiffusive dynamics for the protein [17]. L. Stagg studied the influence of crowders on the stability of native protein both experimentally and theoretically, finding that hard-sphere obstacles can enhance the stability of *Desulfovibrio desulfuricans* flavodoxin [18]. C. Rienzo *et al.* [19] measured protein motion at the unprecedented timescale of 1 μs, finding that the suppression of Brownian motion above some special scale is due to the relatively immobile structures rather than the diffusion crowding agents. It was also demonstrated that crowding agents, especially the immobile ones, can influence dramatically long-time diffusion behavior of substances [20–22], and further biological functions such as signal transduction [23,24], genetic transcription [25], and metabolism [26,27] in cell. While many experimental works have devoted to understand the reaction and diffusion dynamics of macromolecules and polymers in crowded media, theoretical ones are relatively rare except for a few expensive simulation studies.

Very recently, an important theoretical framework based on MCT has been proposed [28–30] by V. Krakoviack to study the glass transition dynamics, as well as the dynamics of a tagged particle in disordered porous media. The system contains fluid particles and matrix particles, and the latter are immobile such that translational invariance is violated. Related equilibrium and dynamic properties of the system must then be split into connected and blocked parts, which serves as the most nontrivial feature of the porous media compared to a normal one. The authors were able to develop the MCT equations for the connected part of the collective and single-particle scattering function, which facilitates one to study the crowded effects. For instance, Krakoviack found that the glass transition point depends strongly on the volume fraction of the matrix particles, and there exists a reentrance phenomenon that is not present in normal dense fluids [29]. A new localized state for a single tagged particle was also found [30]. It is worthy to note here that such a MCT theory for porous media not only can be used to study glass transition behavior, but also serves as a general framework to calculate the coherent and incoherent dynamic scattering functions, which can be very useful for the studies of transport properties in the system.

In the present work, we have tried to study the dynamics of a RC in a porous media, by applying the MCT approach. Our motivation is to help understand the diffusion and conformational dynamics of macromolecules or polymers in crowded systems. Surely, RC is much simpler than real polymer, however, it serves as a basic model and may provide helpful physical insights. We use a bead-spring model to describe the RC, the dynamics of each bead is governed by a GLE with a homogeneous friction kernel $\zeta(t)$. Microscopically, the friction kernel mainly results from the density fluctuations of the media, which make it possible for us to get the expression for $\zeta(t)$ where the equilibrium structures and dynamic scattering

*zhaonanr@scu.edu.cn
†hzhlj@ustc.edu.cn

functions of the porous media are involved. The key step is then to use the MCT for porous media to calculate the scattering functions. With this combined scheme of GLE plus MCT, we are able to study the diffusion dynamics and end-to-end distance fluctuations of the RC, paying particular attention to the effects of crowding [3,4,9,10,14,15,20,27]. The results show that D_{CM} of RC decreases with increasing the media particles which is influenced by matrix more obviously than by fluid. We find that the continuum approximation, which could be used to derive the scaling relation between chain length and D_{CM}, is still valid even for highly crowded environment and short chains. Provided the chain length is long enough, the ACF of end-to-end distance fluctuation shows a clear-cut power-law decaying regime which is of nearly fixed length in logarithmic scale yet it shifts to longer time range, no matter how crowded the environment is. We have also investigated the differences between the fluid-matrix case and the pure fluid case, finding that the lack of translational invariance in space is the main reason resulting in the long time tail in the friction kernel. Compared to direct molecular dynamics (MD) or other mesoscopic simulation methods, our method is much more efficient, systematic, and easier to be extended to other models.

We would like to note here that the problem of polymer chain in an environment of fixed obstacles has a long history in polymer physics since it was a starting point to study entanglement effects. The dynamics of such chains have been discussed in Ref. [31] and have been investigated with experimental, simulation, and theoretical tools. In the pioneer work of de Gennes [32], the polymer motion in such an environment was described by the reptation dynamics, wherein the only allowed motions for the chain are associated with the displacement of certain "defects" along the chain. For such reptation dynamics, the overall diffusion coefficient of the chain is much slower than that predicted by Rouse dynamics. In our present work, we have assumed that the chain follows Rouse dynamics, wherein excluded volume effects are disregarded, and the reptation dynamics is not accounted for. The effects of the crowded media, containing both fixed matrix particles and mobile fluid particles, are combined into the memory friction kernel $\zeta(t)$. This might be applicable if the chain length is not large and the volume fraction of fixed matrix particles is small, such that the chain does not feel strong tube constraints. Certainly, such a simplified model may not describe the real dynamics of macromolecules in crowded environments, however, it serves as a starting point. In addition, our MCT plus GLE framework presents a promising microscopic approach to study such a problem of general interest.

The remainder of the paper is organized as follows. In Sec. II, we introduce our model and theory, including the static structure factor, RC in porous media, and the MCT theory for the time-dependent friction kernel $\zeta(t)$. The relevant physics quantities were calculated numerically in Sec. III followed by conclusions in Sec. IV.

II. MODEL AND THEORY

A. Fluid in porous media

In this section, we discuss the main features of a fluid system in a porous media as shown in Fig. 1. The system

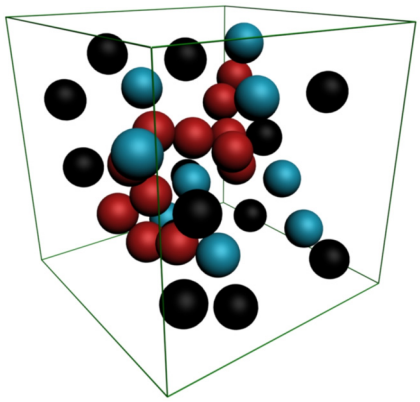

FIG. 1. Sketch of porous model. The black (blue) spheres represent for matrix (fluid) particles which are immobile (mobile). The red spheres represent for the Rouse chain.

contains matrix particles (black balls) and fluid particles (blue balls), the numbers of which are given by N_m and N_f, respectively. The positions of the quenched particles are given by $\{\mathbf{r}_j^m, j = 1, \ldots, N_m\}$, and the time-dependent positions of the fluid particles are denoted by $\{\mathbf{r}_l^f(t), l = 1, \ldots, N_f\}$. The frozen density fluctuations of the immobile matrix particles are given by

$$\rho_{\mathbf{q}}^m = \sum_{j=1}^{N_m} e^{i\mathbf{q}\cdot\mathbf{r}_j^m}, \tag{1}$$

where $\mathbf{q}$ is the wave vector and those of the fluid component are

$$\rho_{\mathbf{q}}^f(t) = \sum_{j=1}^{N_f} e^{i\mathbf{q}\cdot\mathbf{r}_j^f(t)}. \tag{2}$$

Note that the quenched component is static and the density fluctuations do not change with time for a given matrix configuration.

The major difference of this quenched-annealed (QA) mixture with an ordinary binary mixture is that the fluid system has translational and rotational invariance [29]. As a result, the equilibrium average density fluctuation of the fluid component is not zero, i.e., $\langle \rho_{\mathbf{q}}^f \rangle \neq 0$, where $\langle \cdots \rangle$ stands for equilibrium averaging for a certain realization of the disordered matrix. It is only after averaging over disorder that the symmetry is restored such that $\overline{\langle \rho_{\mathbf{q}}^f \rangle} = 0$, and here $\overline{\cdots}$ denotes averaging over the disorder realizations. One then has to consider both relaxing and nonrelaxing part of fluid density fluctuations, given by $\delta\rho_{\mathbf{q}}^f(t) = \rho_{\mathbf{q}}^f(t) - \langle \rho_{\mathbf{q}}^f \rangle$ and $\langle \rho_{\mathbf{q}}^f \rangle$, respectively.

For the static properties of the system, one can define structure factors as follows:

$$S_q^{mm} = \frac{1}{N_m} \overline{\rho_{\mathbf{q}}^m \rho_{-\mathbf{q}}^m}, \tag{3}$$

$$S_q^{ff} = \frac{1}{N_f} \overline{\langle \rho_{\mathbf{q}}^f \rho_{-\mathbf{q}}^f \rangle}, \tag{4}$$

$$S_q^{fm} = \frac{1}{\sqrt{N_f N_m}} \overline{\langle \rho_{\mathbf{q}}^f \rho_{-\mathbf{q}}^m \rangle}. \tag{5}$$

Since $\langle \rho_{\mathbf{q}}^f \rangle \neq 0$, the fluid structure factor S_q^{ff} can be divided into so-called *connected* and *blocked* parts,

$$S_q^{(ff)c} = \frac{1}{N_f} \overline{\langle \delta\rho_{\mathbf{q}}^f \delta\rho_{-\mathbf{q}}^f \rangle} \tag{6}$$

and

$$S_q^{(ff)b} = \frac{1}{N_f} \overline{\langle \rho_{\mathbf{q}}^f \rangle \langle \rho_{-\mathbf{q}}^f \rangle}. \tag{7}$$

Clearly, $S_q^{ff} = S_q^{(ff)c} + S_q^{(ff)b}$.

This splitting of structure factor is well known from the replica theory of QA systems, and one can use the replica Ornstein-Zernike (OZ) equations [29,30] to obtain such properties.

B. Rouse chain in porous media

We now consider an idealized RC containing M beads of mass m_c connected by harmonic springs with frequency ω. The configuration of the chain can be described by a vector $\mathbf{R} = (\mathbf{r}_1, \mathbf{r}_2, \cdots, \mathbf{r}_M)$, where $\mathbf{r}_j$ denotes the displacement vector of the jth bead from its equilibrium position. In the overdamped limit, the dynamics of $\mathbf{R}$ can be described by the following coupled generalized Langevin equations (GLEs):

$$\int_0^t d\tau \zeta(t-\tau) \frac{d\mathbf{r}_j(\tau)}{d\tau} = m_c\omega^2(\mathbf{r}_{j-1} + \mathbf{r}_{j+1} - 2\mathbf{r}_j) + \mathbf{f}_j(t), \tag{8}$$

where $\zeta(t)$ is the friction kernel, which is related to the random force $\mathbf{f}_j(t)$ via fluctuation-theorem,

$$\left\langle f_i^{\mu}(t) f_j^{\nu}(\tau) \right\rangle = k_B T \zeta(t-\tau) \delta_{ij} \delta^{\mu\nu}, \tag{9}$$

with μ and ν represent x, y, or z in cartesian coordinate system. Note that free boundary condition is used in Eq. (8); i.e., $\mathbf{r}_0 = w\mathbf{r}_1$ and $\mathbf{r}_M = \mathbf{r}_{M+1}$ are adopted. The friction kernel is assumed to be determined by the surrounding porous media and thus should be the same for all the beads.

One should note here that the above GLE differs from the standard Rouse dynamics by the inclusion of memory effects in the friction kernel $\zeta(t)$. Nevertheless, the friction kernel is still local, and hydrodynamic interactions (HI) are disregarded. It is generally accepted that HI is important for polymers in dilute solutions, and one should use Zimm model [33] instead of Rouse model to describe the dynamics. In the present work, we are mainly interested in the high-density region, where the total volume fraction of fluid and matrix particles is large and the system is close to the boundary of localized or glassy state, to highlight the effect of crowded environment. In such a dense system, HI may not play a dominant role. It is interesting to take into account HI within the GLE framework, wherein $\zeta(t)$ should then be replaced by a matrix $\zeta_{ij}(t)$. However, how to obtain such a complex matrix $\zeta_{ij}(t)$ from the MCT framework is hard to answer.

We are interested in the diffusion behavior of the whole chain. The diffusion coefficient of the center-of-mass (CM) is given by

$$D_{\mathrm{CM}} = \lim_{t\to\infty} \frac{1}{6t} \Delta^2 \mathbf{r}_{\mathrm{CM}}(t) \equiv \lim_{t\to\infty} \frac{1}{6t} \langle [\mathbf{r}_{\mathrm{CM}}(t) - \mathbf{r}_{\mathrm{CM}}(0)]^2 \rangle, \tag{10}$$

where $\mathbf{r}_{\mathrm{CM}}$ is position vector of the CM,

$$\mathbf{r}_{\mathrm{CM}}(t) = \frac{1}{M} \sum_{i=1}^{M} \mathbf{r}_i(t).$$

In the continuum limit, it can be proved that

$$\Delta^2 \mathbf{r}_{\mathrm{CM}}(t) = \langle [\mathbf{r}_{\mathrm{CM}}(t) - \mathbf{r}_{\mathrm{CM}}(0)]^2 \rangle = \frac{3k_B T}{M} \int_0^t \int_0^t \zeta(t_1 - t_2) \chi(t_1) \chi(t_2) dt_1 dt_2, \tag{11}$$

where $\chi(t)$ is the inverse Laplace transform of $[s\tilde{\zeta}(s)]^{-1}$ with $\tilde{\zeta}(s)$ the Laplace transform of the friction kernel $\zeta(t)$. Clearly, $\Delta^2 \mathbf{r}_{\mathrm{CM}}(t)$ is proportional to M^{-1} in this limit, and hence D_{CM} should also be proportional to M^{-1}. If M is small, the continuum approximation is not applicable and Eq. (11) may not hold. In this case, one must calculate D_{CM} by direct simulation. Surely, one must know the exact form of the kernel $\zeta(t)$. Note that for the standard Rouse model, the noise is white and $\zeta(t)$ is a δ function, i.e., $\zeta(t) = 2\zeta_0\delta(t)$. In this case, $\tilde{\zeta}(s) = 2\zeta_0$ and one easily has $\Delta^2 \mathbf{r}_{\mathrm{CM}}(t) = 6k_B T t/M\zeta_0$ such that $D_{\mathrm{CM}} = k_B T/M\zeta_0$, which is just M^{-1} of the diffusion coefficient of an isolated monomer.

For the RC, another relevant dynamic variable is the distance fluctuation, which can be described by the following auto-correlation function:

$$C_{\mathrm{DF}}(t) = \langle \delta\mathbf{d}(t) \cdot \delta\mathbf{d}(0) \rangle, \tag{12}$$

where $\mathbf{d}(t) = \mathbf{r}_M(t) - \mathbf{r}_1(t)$ is the distance vector between the two ends of the chain, and $\delta\mathbf{d}(t)$ is the deviation of $\mathbf{d}(t)$ from its equilibrium value. For an ideal RC, the analytical expression for this auto-correlation function in the Laplace domain can be obtained [34,35],

$$\tilde{C}_{\mathrm{DF}}(s) = C_{\mathrm{DF}}(0) \sum_{j=\mathrm{odd}}^{M-1} \frac{2}{M} \cos^2\left(\frac{j\pi}{M}\right) \times \left[s + \frac{4\omega^2 m_c}{\tilde{\zeta}(s)} \sin^2\left(\frac{j\pi}{2M}\right) \right]^{-1}, \tag{13}$$

where $C_{\mathrm{DF}}(0) = k_B T/m_c\omega^2$ is the initial value of $C_{\mathrm{DF}}(t)$. One can then perform inverse Laplace transformation to get $C_{\mathrm{DF}}(t)$. Again, one must know the friction kernel $\zeta(t)$ to calculate $C_{\mathrm{DF}}(t)$.

In the case of δ-correlation friction kernel $\zeta(t) = 2\zeta_0\delta(t)$, one can obtain an analytical expression for the correlation function as

$$\frac{C_{\mathrm{DF}}(t)}{C_{\mathrm{DF}}(0)} = \sum_{j=\mathrm{odd}}^{M-1} \frac{2}{M} \cos^2\left(\frac{j\pi}{M}\right) \exp\left[-\Gamma \sin^2\left(\frac{j\pi}{2M}\right) t \right],$$

with $\Gamma = 4\omega^2 m_c/\zeta_0$. In the limit of large M, this expression becomes

$$C_{\mathrm{DF}}(t)/C_{\mathrm{DF}}(0) = \exp(-\Gamma t/2)[I_0(\Gamma t/2) + I_1(\Gamma t/2)],$$

where $I_p(x)$ is the modified Bessel function of the first kind of order p, which behaves as $I_p(x) \sim \exp(x)/\sqrt{2\pi x}$ for large x. Therefore, for $\Gamma t \gg 1$, one has for the correlation function

$$C_{\mathrm{DF}}(t)/C_{\mathrm{DF}}(0) \simeq t^{-1/2}/\sqrt{\Gamma\pi},$$

showing power-law decay with time. Clearly, the onset time t_{on} for such a power-law region is determined by $1/\Gamma$, which in turn depends on the friction constant ζ_0. One should also note that for such a power-law approximation to hold, $\Gamma t \ll M$ should also be satisfied [34]. Thus, the terminated time of this power-law region may be estimated by $t_{off} \sim M/\Gamma$.

For our present work, $\zeta(t)$ may show long tails and deviate largely from a δ function. In this case, analytical expression for $C_{DF}(t)$ is not available. Nevertheless, our results shown below demonstrate that even for such complex friction kernel with long memory, a clear-cut power-law $t^{-1/2}$ region still exists for $C_{DF}(t)$. The onset time of this power-law region will shift to larger values with the increasing of crowed particles, while the ratio t_{off}/t_{on} seems to keep nearly unchanged.

C. Friction kernel in porous media

As discussed in the last subsection, the friction kernel $\zeta(t)$ plays a crucial role to calculate the dynamic behavior of the RC. By definition, $\zeta(t)$ is related to the time-correlation function of the random force that is exerted on each bead by the surrounding media. In phenomenological models, one may just assume some simple forms of $\zeta(t)$, typically a power-law one to account for non-Markovian characteristics, or even more simpler Dirac δ function for white-noise case. Nevertheless, in complex fluids, the friction kernel $\zeta(t)$ may have rather complicated dependence on time, sometimes corresponding to a bimodal shape in the frequency domain [35,36]. One would expect that $\zeta(t)$ in a porous media should depend strongly on the fraction of the matrix component $N_m/(N_m+N_f)$. However, such an issue has not been investigated before, to the best of our knowledge.

The calculation of $\zeta(t)$ is a rather nontrivial problem. In recent years, a MCT framework [35,37,38] has been proposed to calculate $\zeta(t)$ from microscopic interactions, which has appeared to provide a self-consistent and unified description of the friction both at short-time and the long-time limits. According to such a framework, there exist three sources of the friction: binary collision, coupling to the density fluctuation, and coupling to the transverse current. The binary collision dominates the short-time range of the friction kernel and decays relatively fast. The coupling to the density fluctuation is responsible to the cage effect and has a long-time memory comparable to the decay of the solvent cage. The coupling to the transverse current refers to the back-flow effect where the motion of the tagged particle is coupled with the natural current of the solvent. The former two sources retard the diffusion of the tagged molecule while the last one accelerates it.

Within MCT, the total friction kernel can be written in Laplace domain as [35]

$$\frac{1}{\tilde{\zeta}(s)} = \frac{1}{\tilde{\zeta}_B(s)+\tilde{\zeta}_{\rho\rho}(s)} + \tilde{\zeta}_{TT}(s), \tag{14}$$

where $\tilde{\zeta}_B(s)$ is the short-time part of the friction, which results from the direct binary collision between the bead and the solvent particle, $\tilde{\zeta}_{\rho\rho}(s)$ and $\tilde{\zeta}_{TT}(s)$ are the long time parts of the friction which result from the density fluctuation and transverse current, respectively. In our present work, we consider that the bead is of identical size to the solvent particles, such that the transverse current part becomes insignificant compared to the other two terms [39]. In addition, Eq. (8) describes the motion of the RC in the overdamped limit, wherein the binary collision part $\zeta_B(t)$, which only matters in the short time is also negligible compared to the density fluctuation part $\zeta_{\rho\rho}(t)$. Therefore, for the present purpose, we will simply approximate $\zeta(t)$ as $\zeta_{\rho\rho}(t)$.

$\zeta_{\rho\rho}(t)$ is contributed by the density fluctuation of the solvent particles. By definition, it is given by the zero wave vector (macroscopic) limit [40],

$$\zeta_{\rho\rho}(t) = \lim_{q\to 0} \zeta_{\rho\rho}(\mathbf{q},t), \tag{15}$$

of the wave-vector-dependent friction given by

$$\zeta_{\rho\rho}(\mathbf{q},t) = \frac{k_B T}{3}\overline{\langle \mathbf{F}(\mathbf{q},t)\cdot\mathbf{F}(-\mathbf{q},0)\rangle}. \tag{16}$$

Here $\mathbf{F}(\mathbf{q},t)$ is the Fourier transform of the force density $\mathbf{F}(\mathbf{r},t)$ that is exerted on the bead. For the porous media, the density fluctuation in both the fluid and matrix component would contribute to the force density. As a consequence, $\mathbf{F}(\mathbf{r},t)$ is given by

$$\mathbf{F}(\mathbf{r},t) = -n_s(\mathbf{r},t)\nabla_{\mathbf{r}}\int d\mathbf{r}'\big[c_f^s(\mathbf{r}-\mathbf{r}')\rho_f(\mathbf{r}',t) + c_m^s(\mathbf{r}-\mathbf{r}')\rho_m(\mathbf{r}')\big], \tag{17}$$

where $n_s(\mathbf{r},t)$ represents the density distribution of the beads, $c_f^s(\mathbf{r}-\mathbf{r}')$ and $c_m^s(\mathbf{r}-\mathbf{r}')$ denote, respectively, the direct correlation function among the bead and the fluid-matrix component, $\rho_f(\mathbf{r},t)$ is the time-dependent number density of the fluid, and $\rho_m(\mathbf{r})$ is the static number density of the matrix component. $\nabla_{\mathbf{r}}$ denotes the gradient with respect to the variable $\mathbf{r}$. The integral on the right-hand side defines the effective interaction between the surrounding fluid-matrix particles and the beads.

With this form of force density, one has

$$\mathbf{F}(\mathbf{q},t) = -\int \frac{d\mathbf{k}}{(2\pi)^3} n_s(\mathbf{q}-\mathbf{k},t)(i\mathbf{k})\big[c_k^{sf}\rho_f(\mathbf{k},t)+c_k^{sm}\rho_m(\mathbf{k})\big], \tag{18}$$

where c_k^{sf} and c_k^{sm} are the Fourier transform of $c_f^s(\mathbf{r})$ and $c_m^s(\mathbf{r})$ with wave vector $\mathbf{k}$, respectively. Substituting this into Eqs. (16) and (15), after some straightforward algebra, we can get

$$\zeta_{\rho\rho}(t) = \frac{k_B T n_f}{3}\int \frac{d^3\mathbf{k}}{(2\pi)^3} k^2\big[V_k^{(2)}\Phi_k(t)\phi_k^s(t) + V_k^{(1)}\phi_k^s(t)\big], \tag{19}$$

where $n_f = N_f/V$ is the number density of the fluid component. $\Phi_k(t)$ represents the coherent dynamic scattering function of the fluid,

$$\Phi_k(t) = \frac{\overline{\langle \delta\rho_{\mathbf{k}}^f(t)\delta\rho_{-\mathbf{k}}^f(0)\rangle}}{N_f S_k^{ff(c)}},$$

and

$$\phi_k^s(t) = \overline{\langle \rho_{\mathbf{k}}^s(t)\rho_{-\mathbf{k}}^s(0)\rangle}$$

is the tagged-particle incoherent scattering function. $V_k^{(2)}$ and $V_k^{(1)}$ are vortex functions that are given by

$$V_k^{(2)} = \left[c_k^{sf}\right]^2 S_k^{ff(c)}, \tag{20}$$

and

$$V_k^{(1)} = \left(c_k^{sf}\right)^2 S_k^{ff(b)} + 2\sqrt{\frac{n_m}{n_f}} c_k^{sf} c_k^{sm} S_k^{fm} + \frac{n_m}{n_f}\left(c_k^{sm}\right)^2 S_k^{mm}. \tag{21}$$

Note that in a recent series of papers [28–30], V. Krakoviack has established a MCT framework to study the glass transition behavior in porous media. Therein, the dynamic equation for the tagged-particle scattering function $\phi_k^s(t)$ was obtained within MCT approximations. The memory kernel $M^{\rm mct}(q,t)$ with wave vector $\mathbf{q}$ involved there also contained a quadratic term $V_{\mathbf{q},\mathbf{k}}^{(2)}$ and a linear term $V_{\mathbf{q},\mathbf{k}}^{(1)}$, associated with, respectively, the quadratic mode $\phi_k^s(t)\Phi_{|\mathbf{q}-\mathbf{k}|}(t)$ and single mode $\phi_k^s(t)$. Actually, the friction kernel $\zeta_{\rho\rho}(t)$ considered in the present paper is closely related with the memory kernel $M^{\rm mct}(q,t)$, i.e., $\zeta_{\rho\rho}(t) \propto \lim_{q\to 0} M^{\rm mct}(q,t)$. The results obtained here are based on a relatively "naive" version of MCT, i.e., the projected random force density on the tagged particle is simply replaced by the total force density $F(\mathbf{r},t)$ defined through the direct correlation functions. In Ref. [30], a more subtle method was used, which projected the random force to the product of density fluctuation modes containing both of fluids and matrices. The result here for $V_k^{(2)}$ is the same as that obtained in Ref. [30], while that for $V_k^{(1)}$ is a little different. Nevertheless, as discussed in detail in Ref. [30], such a difference is actually negligible given that the so-called blocked part of the direct correlation function can be ignored, which is a generally acceptable approximation in porous media.

D. Scattering functions in porous media

In Sec. II C, we have obtained the formula to calculate the friction kernel $\zeta(t)$ in the long-time limit, which for simplicity is given by the density fluctuation part $\zeta_{\rho\rho}(t)$, described in Eq. (19). However, to calculate $\zeta_{\rho\rho}(t)$, one must know the k-dependent scattering functions (or density correlators) $\Phi_k(t)$ and $\phi_k^s(t)$ of the surrounding fluid in the porous media. In previous works, one generally used approximations for such two correlators, for instance, viscoelastic approximation for $\Phi_k(t)$ or Gaussian approximation for $\phi_k^s(t)$ [39,41]. Since such approximations usually involve the long time transport coefficients such as the diffusion constant or viscosity as input, while these coefficients are often what we want to calculate, this framework must be done in a self-consistent manner. Nevertheless, for fluids in porous media, the validity of such approximations is not well justified, which renders the self-consistent calculation of $\zeta_{\rho\rho}(t)$ not quite applicable.

In the present work, we will calculate the scattering functions $\Phi_q(t)$ and $\phi_q^s(t)$ in a more straightforward manner, by using the MCT formalism proposed by V. Krakoviack, already mentioned in last subsection. In Refs. [28–30], V. Krakoviack had developed the equations governing the evolution of $\Phi_q(t)$ and $\phi_q^s(t)$ for the fluid component in porous media, assuming that the slow dynamics of the fluid is dominated by three types of coupled modes, $\delta\rho_{\mathbf{k}}^f \delta\rho_{\mathbf{q}-\mathbf{k}}^f$, $\delta\rho_{\mathbf{k}}^f \rho_{\mathbf{q}-\mathbf{k}}^m$, and $\delta\rho_{\mathbf{k}}^f \langle\rho_{\mathbf{q}-\mathbf{k}}^f\rangle$. Here we only quote the final results and the readers may turn to the references for details. In the overdamped limit, the generalized relaxation equation for $\Phi_q(t)$ reads

$$\tau_q^c \dot{\Phi}_q(t) + \Phi_q(t) + \int_0^t d\tau m_q(t-\tau)\dot{\Phi}_q(\tau) = 0, \tag{22}$$

where τ_q^c is a short-time scale related to the coherent motion, which will be given below, and the q-dependent memory kernel $m_q(t)$ is given by

$$m_q(t) = \int \frac{d^3\mathbf{k}}{(2\pi)^3}\left[V_{\mathbf{q},\mathbf{k}}^{(2)}\Phi_k(t)\Phi_{|\mathbf{q}-\mathbf{k}|}(t) + V_{\mathbf{q},\mathbf{k}}^{(1)}\Phi_k(t)\right], \tag{23}$$

with the quadratic vortex function,

$$V_{\mathbf{q},\mathbf{k}}^{(2)} = \frac{1}{2} n_f S_q^{(ff)c}\left[\frac{(\mathbf{q}\cdot\mathbf{k})}{q^2} c_k^{(ff)c} + \frac{\mathbf{q}\cdot(\mathbf{q}-\mathbf{k})}{q^2} c_{|\mathbf{q}-\mathbf{k}|}^{(ff)c}\right]^2 S_k^{(ff)c} S_{|\mathbf{q}-\mathbf{k}|}^{(ff)c}, \tag{24}$$

and linear vortex function,

$$V_{\mathbf{q},\mathbf{k}}^{(1)} = n_f S_q^{(ff)c}\left[\frac{(\mathbf{q}\cdot\mathbf{k})}{q^2} c_k^{(ff)c} + \frac{1}{n_f}\frac{\mathbf{q}\cdot(\mathbf{q}-\mathbf{k})}{q^2}\right]^2 S_k^{(ff)c} S_{|\mathbf{q}-\mathbf{k}|}^{(ff)b}. \tag{25}$$

Herein, $c_k^{ff(c)}$ denotes the connected-part of the direct correlation function between the fluid particles. Similarly, the tagged-particle density correlator $\phi_q^s(t)$ also satisfies a generalized relaxation equation,

$$\tau_q^s \dot{\phi}_q^s(t) + \phi_q^s(t) + \int_0^t d\tau m_q^s(t-\tau)\dot{\phi}_q^s(\tau) = 0, \tag{26}$$

where τ_q^s is also a short-time scale related to the tagged particle motion and the memory kernel $m_q^s(t)$ is given by

$$m_q^s(t) = \int \frac{d^3\mathbf{k}}{(2\pi)^3}\left[V_{\mathbf{q},\mathbf{k}}^{s(2)}\phi_k^s(t)\Phi_{|\mathbf{q}-\mathbf{k}|}(t) + V_{\mathbf{q},\mathbf{k}}^{s(1)}\phi_k^s(t)\right], \tag{27}$$

with the vortex functions,

$$V_{\mathbf{q},\mathbf{k}}^{s(2)} = n_f\left[\frac{\mathbf{q}\cdot(\mathbf{q}-\mathbf{k})}{q^2} c_{|\mathbf{q}-\mathbf{k}|}^{sf(c)}\right]^2 S_{|\mathbf{q}-\mathbf{k}|}^{ff(c)} \tag{28}$$

and

$$V_{\mathbf{q},\mathbf{k}}^{s(1)} = \left[\frac{\mathbf{q}\cdot(\mathbf{q}-\mathbf{k})}{q^2}\right]^2 h_{|\mathbf{q}-\mathbf{k}|}^{ss(b)}, \tag{29}$$

where $c_k^{sf(c)}$is the connected part of the direct correlation function between the tagged particle and fluid particles, $h_q^{ss(b)}$ is the blocked part of the total correlation function among tagged particles. Note that after taking the limit $q \to 0$, $V_{\mathbf{q},\mathbf{k}}^{s(2)}$ becomes coincident with the vortex $V_k^{(2)}$ used in $\zeta_{\rho\rho}(t)$, Eq. (20). One can also show that in this limit, $V_{\mathbf{q},\mathbf{k}}^{s(1)}$ is also consistent with

Eq. (21) given that the block part of the direct correlation function can be ignored [30]. In this case, we have [30]

$$h_k^{ss(b)} = \left(c_k^{sf}\right)^2 S_k^{ff(b)} + 2\sqrt{\frac{n_m}{n_f}} c_k^{sf} c_k^{sm} S_k^{fm} + \frac{n_m}{n_f}\left(c_k^{sm}\right)^2 S_k^{mm} = n_f V_k^{(1)}. \quad (30)$$

From Eqs. (22)–(29), one can numerically calculate the coherent density correlator $\phi_q(t)$ as well as the tagged particle correlator $\phi_q^s(t)$, given the static structural properties described in Sec. II A as inputs. Nevertheless, one still needs to specify the two parameters τ_q^c and τ_q^s to perform the numerical calculation. In the literatures [30], the exact value of such parameters were usually not necessary, since they just determine some relative time scales. In the present work, however, we are particularly interested in how the diffusion behavior of the Rouse chain would depend on the volume fraction of the fluid or matrix component (n_f or n_m), these time-scale parameters cannot be chosen arbitrarily. At least, their dependencies on the volume fraction should be accounted for. Written explicitly, the expressions for τ_q^c and τ_q^s are

$$\tau_q^c = \frac{S_q^{ff(c)}}{q^2 D_0} \quad (31)$$

and

$$\tau_q^s = \frac{1}{q^2 D_0^s}, \quad (32)$$

where D_0(or D_0^s) is the short-time diffusion coefficient of a fluid particle or the tagged particle, respectively. In our present work, the tagged particle is of the same size as the fluid particle, such that $D_0 = D_0^s$. Physically, these short-time diffusion constants are mainly decided by the binary collisions. According to the MCT framework proposed by B. Bagchi *et al.*, the calculation of such a binary term is not a trivial task. They must be dependent on the details of the intermolecular interactions on the microscopic level. In the present work, for simplicity, we assume that the fluid-matrix particles and the chain beads are all hard spheres. In this case, one can use the Enskog kinetic theory to estimate the short-time diffusion coefficient of a particle as

$$D_0^\mu = k_B T/\zeta_B^\mu,$$

where ζ_B^μ is the friction coefficient given by

$$\zeta_B^\mu = \frac{16\pi}{3}\left(\frac{k_B T}{2\pi}\right)^{1/2} \sum_\nu \left(\frac{m_\mu m_\nu}{m_\mu + m_\nu}\right)^{1/2} \rho_\nu \sigma_{\mu\nu}^2 g_{\mu\nu}(\sigma_{\mu\nu}), \quad (33)$$

where m_μ and ρ_μ are, respectively, the mass and number density of μ-species, $\sigma_{\mu\nu}$ is the summation of radius of μ and ν particles, $g_{\mu\nu}(r)$ is the partial radial distribution function. The summation runs over all fluid and matrix components.

E. Summary of the method

Here, we will briefly summarize the main scheme we described above for the calculation of the diffusion behavior as well as the distance fluctuation of the RC. First of all, we need to use the replica OZ equation to get the static properties of the system, including the structure factors ($S_k^{(ff)c}$, $S_k^{(ff)b}$, S_k^{fm}, S_k^{mm}), direct correlations functions among the tagged particle and the fluid or matrix particles (c_k^{ff}, c_k^{sf}, c_k^{sm}), and the total correlation function $h_k^{ss(b)}$. Note that in our present work, blocked parts of the direct correlation functions are ignored, such that $c_k^{ff(c)} = c_k^{ff}$, $c_k^{sf(c)} = c_k^{sf}$, and the total correlation function $h_k^{ss(b)}$ equals to $n_f V_k^{(1)}$, as shown in Eq. (30). Second, we use the MCT equations given in Sec. II D to get the k-dependent coherent density correlator $\Phi_k(t)$ and tagged particle correlator $\phi_k^s(t)$ for the fluid component, by adopting the Enskog kinetic theory for the short-time diffusion coefficient D_0. Third, these density correlators are used to calculate the friction kernel $\zeta_{\rho\rho}(t)$, which is finally substituted into the formula for the RC to compute the diffusion constant $D_{\rm CM}$ or distance fluctuation correlation function $C_{\rm DF}(t)$. Note that our scheme does not require any self-consistent calculation. We are mainly interested in how the porous environment would influence these properties. The main results of our work will be presented in the following section.

III. RESULTS AND DISCUSSIONS

Surely, the dynamics in a porous media depends strongly on the volume fractions of the fluid, φ_f, and that of the matrix, φ_m. The phase behavior of a quenched-annealed binary mixture of fluid and matrix particles, both being hard spheres of the same sizes, has been studied in detail in Refs. [29,30]. If both φ_f and φ_m are small, the system remains in liquid state. With the increment of the matrix fraction φ_m, the fluid particles may first become localized and then enter into a glassy state if φ_f is not too large, say, $\varphi_f < 0.42$. If $\varphi_f > 0.42$, however, the system may change directly from fluid to glassy state without bypassing a localized state. In the present work, we are mainly interested in the high-density region, where the system is close to the boundary of localized or glassy state, to highlight the effect of crowded environment. We expect that anomalous behaviors resulting from the porous media and their effects on the dynamics of RC can be clearly demonstrated. Note that all the static properties, including the direct and total pair correlation functions, structure factors, etc., are obtained by solving the replica OZ equations as those described in the appendices of Refs. [29,30].

As already discussed in the end of the last section, we first need to obtain the short-time diffusion coefficient D_0. Basically, D_0 decreases with increasing φ_f or φ_m. In Fig. 2, the dependence of D_0 as a function of φ_f for fixed φ_m (bottom and left, black line), or of φ_m for fixed φ_f (up and right, red line) is drawn. For the data considered here, we see that D_0 shows power-law decaying with φ_f when the matrix volume fraction is small (here $\varphi_m = 0.0524$, corresponding to a number density of matrix particles $n_m = 0.1$ since $\varphi = \frac{n\pi d^3}{6}$). Nevertheless, such a power-law dependence is not observed among D_0 and φ_m for $\varphi_f = 0.419$ (corresponding $n_f = 0.8$). In the inset of Fig. 2, we show the dependence of D_0 on φ_m while keeping the total volume fraction $\varphi_m + \varphi_f$ fixed. Clearly, D_0 decreases monotonically as φ_m increases, i.e., when more and more fluid particles are replaced by the matrix ones under fixed volume

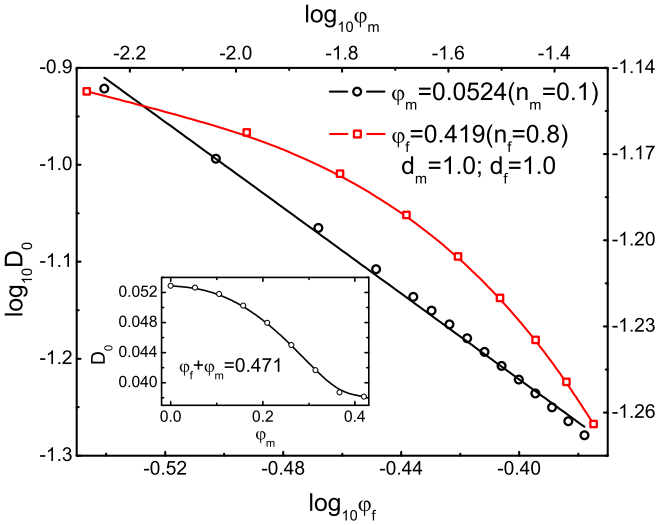

FIG. 2. Short-time diffusion coefficient D_0 vs. φ_f and φ_m in logarithm scales. The black and red lines are corresponding to the left and right axis and fixing $\varphi_m = 0.0524$ and $\varphi_f = 0.419$, respectively. d_f and d_m denote the diameters of fluid and matrix particles, respectively.

fraction, the short-time diffusion of fluid particle gradually slower. This indicates that matrix and fluid particles take rather different effects on the short-time diffusion behavior of the tagged particle, as one can expect.

With the calculated D_0, one can then obtain the scattering functions $\Phi_k(t)$ and $\phi_k^s(t)$, using the methods described in detail in the Sec. II D. As an example, the results for $\varphi_m = 0.0524$ under various φ_f are depicted in Fig. 3. If φ_f is relatively small, both $\Phi_k(t)$ and $\phi_k^s(t)$ decrease fast to zero with time, indicating that the system remains in a fluid state. With increasing φ_f, the system becomes more and more crowded, such that the relaxation time of both scattering functions become larger and larger. If φ_f exceeds some threshold value, for instance $\varphi_f = 0.424$ here, an obvious plateau with nonzero value of $\Phi_k(t \to \infty)$ or $\phi_k^s(t \to \infty)$ appears, indicating that the system enters nonergodic glassy-like state, wherein the viscosity of the system diverges and the long-time diffusion coefficient of the tagged particle becomes zero.

We note here that the volume fraction $\varphi_m = 0.0524$ is not large. In this case, the system is not filled with too many immobile matrix particles, and $\Phi_k(t)$ and $\phi_k^s(t)$ behave rather similarly. However, if φ_m becomes larger, $\phi_k^s(t)$ and $\Phi_k(t)$ may show totally different behaviors. For instance, for $\varphi_m = 0.157(n_m = 0.3)$ and $\varphi_f = 0.209(n_f = 0.4)$, as also shown in Fig. 3 by the dash-dot lines, one can see that the $\Phi_k(t)$ will finally relax to zero, indicating that the system behaves collectively as a fluid state, while $\phi_k^s(t)$ decays to a nonzero plateau, indicating that a single tagged particle gets trapped into a localized state [30]. This localized state will lead to the disappearance of the long-time diffusion constant for a tagged particle. Since we are interested in the diffusion behavior of a RC, wherein each bead can be viewed as a tagged particle in the present context, we will mainly focus on the parameter region where this localized state does not occur. Thus, in the following parts, the volume fraction of the matrix particles φ_m will be set to be smaller than 0.0524 (corresponding to a number fraction $n_m = 0.1$), and φ_f will be kept below the glass-transition point, say, smaller than 0.419 (corresponding to $n_f = 0.8$) if not otherwise stated.

With $\Phi_k(t)$ and $\phi_k^s(t)$ obtained above, one can get the friction kernel $\zeta_{\rho\rho}(t)$ according to Eq. (19), which enters Eq. (8) as $\zeta(t)$. For instances, Fig. 4 shows the time-dependencies of $\zeta(t)$ for several difference values of φ_f with fixed $\varphi_m = 0.0524$. Clearly, the kernel becomes larger and spans a wider time-range with the increment of φ_f. We note that the integrated area under the curve of $\zeta(t)$, i.e., $\zeta_0 = \int_0^\infty \zeta(t)dt$, qualitatively measures the effective friction coefficient for the tagged particle. Hence, the average friction that is experienced by a bead becomes larger in a higher volume fraction as expected. In addition, if the volume fraction approaches the glass-forming value, the system would get much more crowded and the friction kernel shows a rather significant long tail, as shown in Fig. 4 for $\varphi_f = 0.419$. As already discussed in many literatures, such a long tail is due to the cage effects

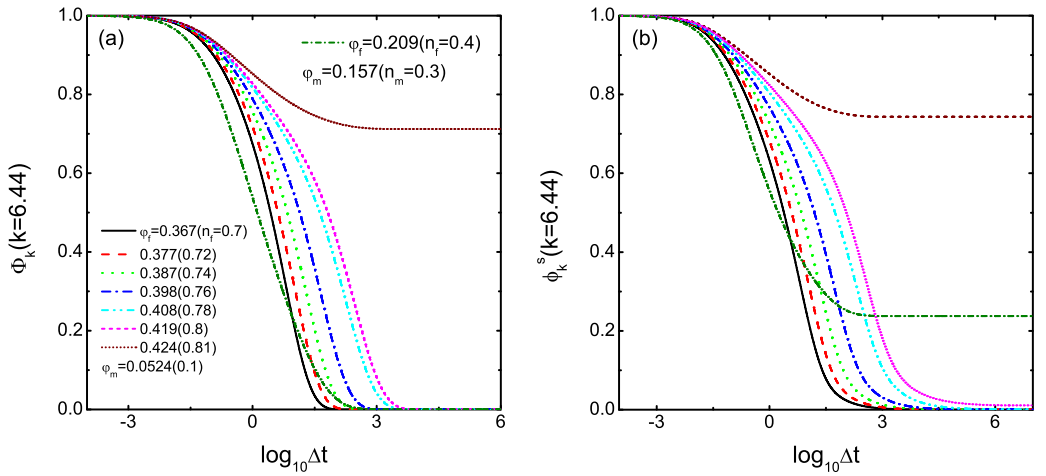

FIG. 3. The scattering functions $\Phi_k(t)$ and $\phi_k^s(t)$. The lines of same color in (a) and (b) are corresponding to the same volume fraction systems. $k = 6.44$ is the frequency space position of the first peak of $S_k^{ff(c)}$. The dash-dot line is the system with $\varphi_f = 0.209$ and $\varphi_m = 0.157$. In this situation, system enters localized state due to the influence of matrix, which is reflected by the plateau of $\phi_k^s(t)$.

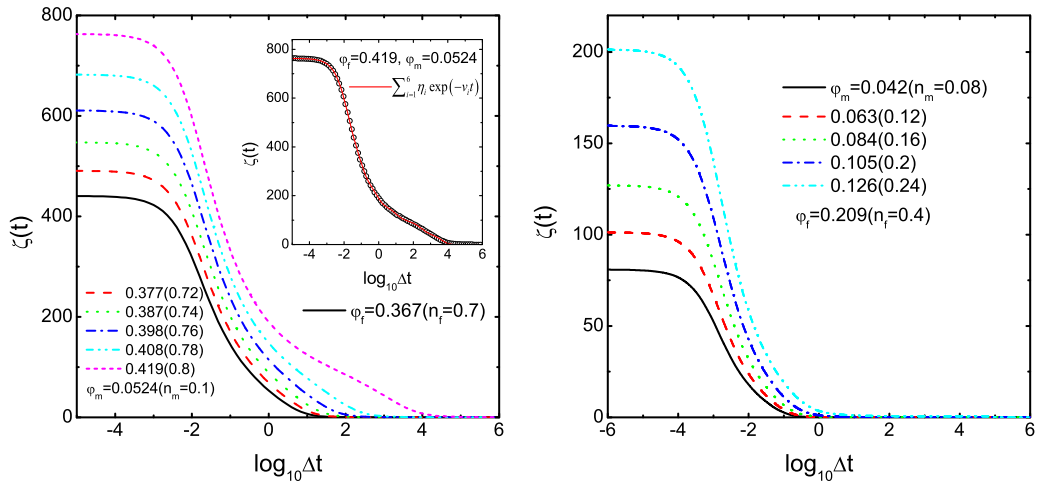

FIG. 4. Friction kernel ζ vs. t in logarithmic space. The volume fraction of matrix φ_m is fixed at 0.0524. The multiexponential fitting is shown in the inset. The open circle are the data obtained from calculating. And the red line is the fitting curve $\sum_{i=1}^{6} \eta_i \exp(-v_i t)$, the fitting is very well in almost 11 order of magnitudes.

resulting from the surrounding fluid particles in a dense system and would lead to anomalous diffusive behavior of the tagged particle in the related time range characterized by the relaxation time τ of $\zeta(t)$. Only for time much larger than τ, the memory effects lose and the particle would undergo a normal diffusion. Interestingly, the friction kernel shows a clear multi-exponential feature, i.e., it can be well-fitted by the summation of several single-exponential decaying functions [42]. As an example, the inset of Fig. 4 shows the fitting of $\zeta(t)$ for $\varphi_f = 0.419$ by using six single-exponential functions.

We are now ready to investigate the dynamics of the RC by using the GLE Eq. (8). First of all, we are interested in the overall diffusion coefficient of CM of the chain. The mean-square displacements (MSDs) of the CM, $\langle \Delta^2 \mathbf{r}_{\rm CM}(t) \rangle$, at different fluid or matrix densities are shown in Fig. 5. Clearly, the MSD increases linearly with time for small t, indicating that the chain undergoes a normal diffusive behavior. In the long-time limit, the slopes of the lines with time are also nearly one, i.e., the chain also shows normal diffusion as well. Nevertheless, the chain exhibits obvious subdiffusion in the intermediate time range, especially for high densities of fluid or matrix. For instance, for $\varphi_f = 0.419$, which is close to the glass-forming point, the system enters the subdiffusion region at $t = t_1 \simeq 10^{-2}$ and gets trapped in a very small space region (the MSD increases little) for a very long time until the chain shows normal diffusion again for $t > t_2 \simeq 10^4$. Such an anomalous diffusion is due to the cage effects, and the time length $t_2 - t_1$ qualitatively measures the average waiting time that the chain escape from the cage. Note the onset time t_2 nearly coincides with the time that $\zeta(t)$ relaxes to zero, see Fig. 4. The long-time diffusion coefficient $D_{\rm CM}$ can be obtained via Eq. (10). Surely, $D_{\rm CM}$ will decrease with the increment of φ_f or φ_m, as shown in the insets of Fig. 5. For the parameter value considered here, for instance $\varphi_m = 0.0524$ with varying φ_f, $D_{\rm CM}$ nearly decays as $\exp(-\gamma\varphi_f)$ with γ a certain constant for $\varphi_f < 0.40$, after which it decreases very fast upon approaching the localization state. This is also the case if φ_f is fixed with varying φ_m as shown in the inset of Fig. 5(b).

In Ref. [43], A. J. Monero and J. Colmenero performed simulations for a simple model of polymer blends by introducing an A-B mixture of bead-spring chains. They used LJ potential for monomer-monomer interactions and finitely extensible nonlinear elastic potential for chain connectivity. The interaction diameter for B monomers is smaller than that for A ones, such that B is a fast component and A is relatively slow. The authors analyzed the dynamics of the chains via Rouse modes. They found that while the slow component A showed typical Rouse dynamics, the fast one B showed large deviations from exponentiality, which could be associated with strong memory effects induced by the slow nature of the confining matrix formed by A components. Such an anomalous behavior becomes more apparent with increasing of the dynamic asymmetry of the system or decreasing temperature T. We find that the strong memory effects found in this reference work is much related to our present work. In Fig. 5 of our paper, the MSD also shows strong anomalous region with time, with the exponent decreases with increasing φ_f or φ_m, as demonstrated by the new insets in Fig. 5. In Refs. [44–46], Yethiraj group studied the structure and dynamics of polymer chains in porous media by using simulations as well as integral equation theory. In particular, they have developed the replica polymer reference interaction site model (PRISM) method to study the swelling of polymer chains in porous media, finding that the radius of gyration (R_g) shows nonmonotonic dependence on the volume fraction of matrix particles [44,46]. More interestingly, they had used molecular dynamics simulations to study the diffusion $D_{\rm CM}$ of the chain, finding that the scaling of $D_{\rm CM}$ with M is stronger than M^{-1} in the presence of matrix particles with $\varphi_m = 0.1$, which is at variance with the Rouse model prediction. This seems to suggest the failure of Rouse dynamics to describe the chain dynamics in their system.

As discussed in Sec. II B, given by Eq. (11), $D_{\rm CM}$ should be inversely proportional to the number of total beads M of the RC in the large M limit. In our present work, we only consider short chains with M not larger than a few tens. Therefore, we have performed simulations to study the dependence of

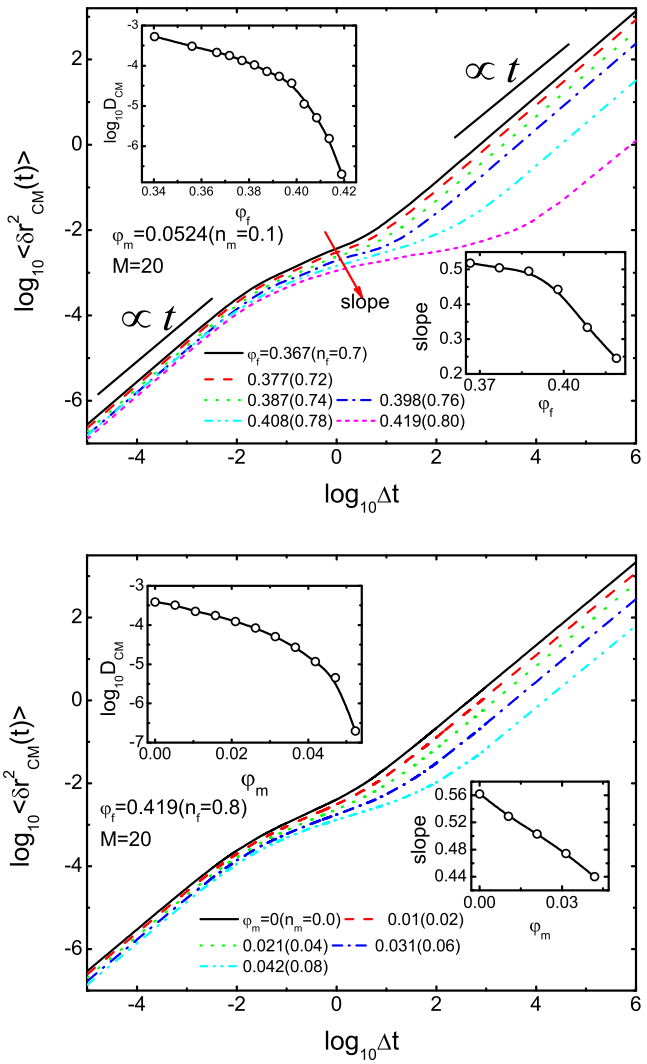

FIG. 5. MSD of rouse chain CM as a function of t with different φ_f and φ_m. Insets: The long-time diffusion coefficient $D_{\rm CM}$ as functions of φ_f and φ_m. The black lines are drawn for guiding eyes. The small insets show the dependencies of the subdiffusion scaling exponent on φ_f or φ_m.

$D_{\rm CM}$ on M in our system. The results are shown in Fig. 6 for fixed φ_m with varying φ_f. Clearly, we find $\log D_{\rm CM} \propto -\log M$ within the statistical errors. Therefore, $D_{\rm CM} \propto M^{-1}$ does hold even for short chains and in porous media. Such a scaling relation is rather robust, even if $D_{\rm CM}$ is very small for high volume fractions of fluid and matrix particles as indicated by the line with $\varphi_f = 0.419$. We note here that such a scaling between $D_{\rm CM}$ and M would still hold for larger fraction of matrix particles φ_m, because the effect of increasing matrix particles has been accounted for in the memory kernel. With increasing φ_m, the friction kernel will show longer tails with longer memory, but the scaling with M would not change given the Rouse dynamics is satisfied. This picture is at variance with some real systems, where increasing fixed obstacles would lead to reptation dynamics such that the diffusion becomes much slower and $D_{\rm CM}$ shows stronger dependence on the chain length as $D_{\rm CM} \sim M^{-2}$ [31,32].

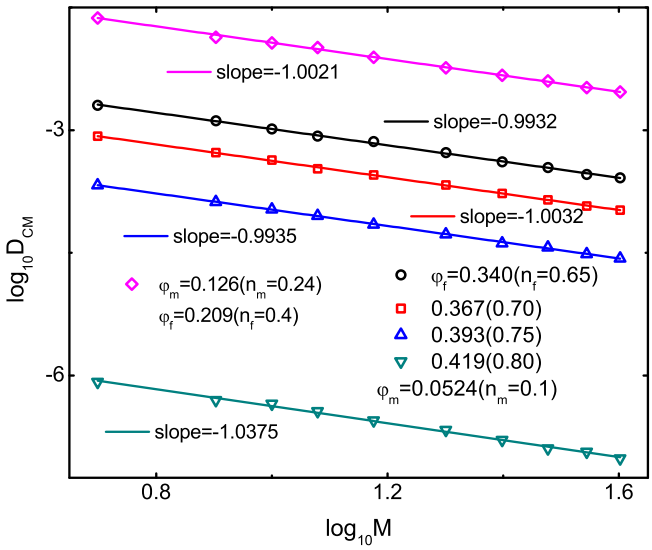

FIG. 6. $D_{\rm CM}$ as functions of bead number M with different φ_f and φ_m. The values of M from left to right are 8, 10, 12, 15, 20, 25, 30, 35, 40. The straight lines are the linear fitting of these data.

Another relevant dynamics of the Rouse chain is about the distance fluctuation characterized by the ACF defined in Eq. (12), which can be calculated conveniently in the Laplace domain by using Eq. (13). Very recently, we have investigated the distance fluctuation of a RC in Lennard-Jones liquid by using similar methods, finding that there always exists a time range from $t_{\rm on}$ to $t_{\rm off}$, wherein $C_{\rm DF}(t)/C_{\rm DF}(0)$ shows robust power law $t^{-0.5}$ with time, given that the chain length is long enough [35]. Herein, we find very similar results in a porous media, although the friction kernel $\zeta(t)$ shows rather nontrivial features. Figure 7(a) shows the dependencies of $C_{\rm DF}(t)/C_{\rm DF}(0)$ with time t for different chain lengths M with fixed φ_f and φ_m. A clear power-law $t^{-0.5}$ region appears if M is not too small. The onset time $t_{\rm on}$ of this power-law region keeps nearly the same for different M, while the end time $t_{\rm off}$ of this region increases with M. Figure 7(b) presents $C_{\rm DF}(t)/C_{\rm DF}(0)$ for different φ_f while keeping φ_m fixed and $M = 200$. With increasing φ_f, both $t_{\rm on}$ and $t_{\rm off}$ increases quickly, while the time interval $\log t_{\rm on} - \log t_{\rm off}$ keeps nearly unchanged, even when the system becomes rather crowding for $\varphi_f = 0.419$. Such an interesting finding is quite similar to that in our previous study [35], as mentioned just above.

A possible understanding of this interesting phenomenon may be as follows. As discussed in Sec. II B, even for δ-correlated friction kernel, one still observes $t^{-1/2}$ region bounded by $1 \ll \Gamma t \ll M$. Thus, the range of this power-law region would generally increase with the chain length M, but not depend on $\Gamma = 4\omega^2/\zeta_0$. It is thus reasonable that the ratio $t_{\rm off}/t_{\rm on}$ remains nearly a constant for different Γ. In the case of GLE, where the kernel has long memory, one may still approximate the kernel by a δ-correlated one at a "coarse-graining" time scale, where this memory has lost. For this coarse-grained model, $t_{\rm off}/t_{\rm on}$ for the power-law region would still be nearly a constant only dependent on the chain length M, but now the absolute values of $t_{\rm on}$ and $t_{\rm off}$ shift and depend on the "effective" friction $\zeta_0^{\rm CG}$, where "CG" stands

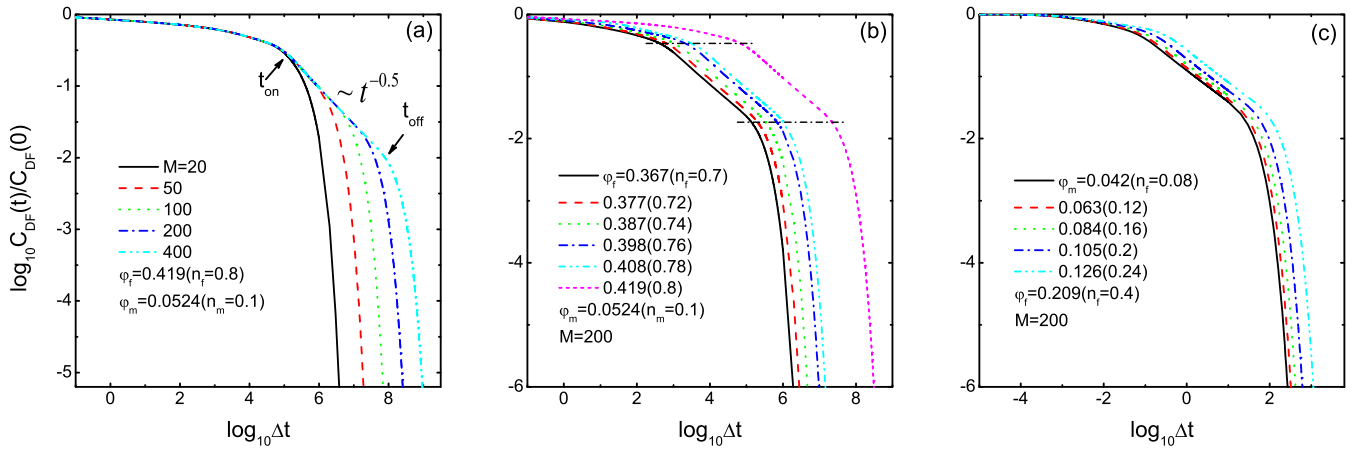

FIG. 7. The distance ACF $C_{\rm DF}(t)/C_{\rm DF}(0)$ as function of t.

for coarse-graining. As shown in Fig. 4, with the increasing of φ_f (φ_m fixed), the relaxation time of the memory kernel $\zeta(t)$ also increases, indicating that the coarse-grained time scale for the system to be nearly δ-correlated increases too. In addition, the total effective friction $\zeta_0^{\rm CG} \propto \int_0^\infty \zeta(t)dt$ also increases with increasing φ_f. These two effects both lead to the right shifts of both $t_{\rm on}$ and $t_{\rm off}$. With more fraction of fixed particles φ_m, the qualitative behavior would be the same as long as the system has not entered the glassy region, since the effect of the matrix has been taken into account by the friction kernel $\zeta(t)$ in the present model. This is demonstrated in Fig. 7(c), where the results for $\varphi_m = 0.1$ have been plotted, and qualitatively very similar behaviors can be observed as those in Fig. 7(b).

Finally, one may ask how the particular feature of the porous media would influence the chain dynamics described above. To answer this question, we may compare the results obtained above, referred to as fluid-matrix (FM) case, with the case wherein the matrix particles are replaced by the fluid particles with the same volume fraction, which may be termed as fluid-fluid (FF) case. To obtain the results for the FF case, one just needs to remove the $V_k^{(1)}$ term in Eq. (19) and set the total volume fraction of fluid particles to be $\varphi_f^{\rm FF} = \varphi_f^{\rm FM} + \varphi_m^{\rm FM}$. Typical results for the friction kernel $\zeta(t)$ are shown in Fig. 8(a) with $\varphi_f^{\rm FF} = 0.471$ and $\varphi_f^{\rm FF} = 0.419$. Clearly, $\zeta(t)$ shows an apparent long tail in the large time limit for the FM case (black line) compared to the FF case (red line). Since the total number of ambient particles are the same for both cases, this difference must be related to the immobile feature of the matrix particles which leads to the lack of translational invariance. We also note that the difference becomes significant only for long times, which means the porous media leads to more pronounced subdiffusion behavior. Correspondingly, results for the center-of-mass diffusion coefficient $D_{\rm CM}$ as a function of $\varphi_f^{\rm FM} + \varphi_m^{\rm FM}$ (with fixed $\varphi_m^{\rm FM} = 0.0524$) or $\varphi_f^{\rm FF}$ (being equal to $\varphi_f^{\rm FM} + \varphi_m^{\rm FM}$) are depicted in Fig. 8(b). As expected, the immobile feature of the matrix component also leads to a reducing of the $D_{\rm CM}$ and a sharper dependence of $D_{\rm CM}$ on the total number of fluid (and matrix) particles. Therefore, proper consideration of the matrix particles is of particular importance for the investigation of the dynamics of any solute in a porous media.

IV. CONCLUSION

In summary, we have studied the long-time diffusion behavior and the end-to-end distance fluctuations of a bead-spring RC dissolved in porous media, by using a GLE wherein the friction kernel $\zeta(t)$ is obtained by kinetic MCT. The porous media contains fluid particles as well as immobile matrix particles, leading to the lack of translational invariance of the system. The main source of the friction kernel $\zeta(t)$ is density fluctuation in the media, containing static or dynamic components. By adopting a simple density-functional approach, we can calculate $\zeta(t)$ directly, given the collective and tagged particle density correlators $\Phi_k(t)$ and $\phi_k(t)$ as inputs. These latter density correlators can be obtained by solving specific MCT equations for porous media, wherein the equilibrium structure factors are obtained by solving replica OZ equations with PY closure. It is found that $\zeta(t)$ exhibits rather complicated features in such porous media. Especially in the high-volume fraction of fluid and matrix, $\zeta(t)$ would show a very long tail due to the cage effect generated by surrounding particles. Substituting $\zeta(t)$ into the GLE for the RC, we can calculate the long-time center-of-mass diffusion constant $D_{\rm CM}$ of the chain. $D_{\rm CM}$ decreases with the increment of media particles as expected, while matrix particles have stronger influences on $D_{\rm CM}$ than the fluid particles. It is found that the scaling relation between chain length M and $D_{\rm CM}$ agreed with the continuum approximation even for both highly crowded environment and very small M. Based on the GLE, we can also calculate $C_Q(t)$, ACF of the end-to-end distance fluctuation, which depends explicitly on the friction kernel $\zeta(t)$. A clear-cut power-law decaying regime shows up in $C_Q(t)$ with a robust exponent to be -0.5, corresponding to subdiffusion behavior of the chain, provided that the chain length is long enough. Interestingly, the power-law region of $C_Q(t)$ has a nearly fixed length in logarithmic scale, but shifts to longer time range, with increasing the total volume fraction of media particles. By comparing the results for the porous media and a hypothetical system, wherein the matrix particles are replaced by fluid particles with the same volume fraction, we find that the lack of translational invariance is the main reason for the long-time tail in $\zeta(t)$. We believe that our work provides a simple but efficient theoretical framework to study transport properties of

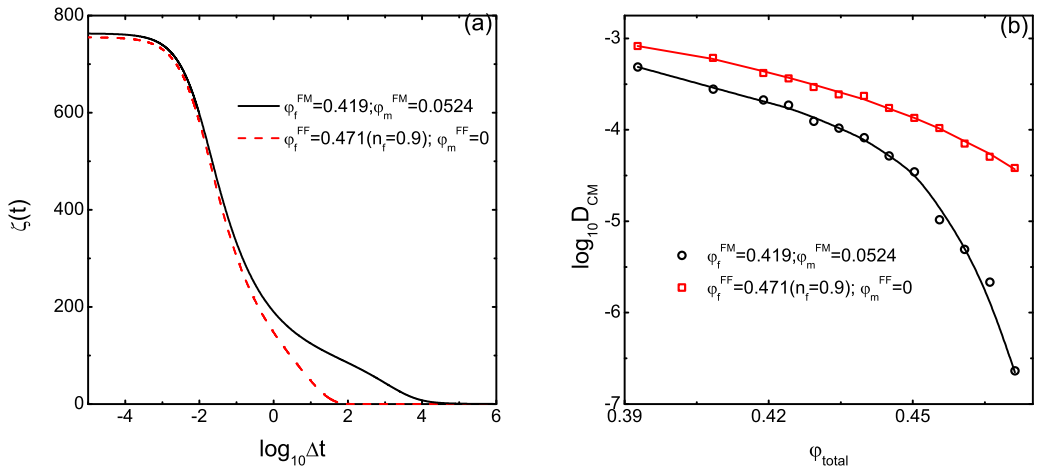

FIG. 8. (a) The black line: fluid-matrix (FM) case. The red line: pure fluid case. (b) D_{CM} as functions of φ_{total} in different cases, where φ_{total} is the total volume fraction of particles including fluid and matrix. The lines are drawn for guiding eyes.

nanoparticles or macromolecules in a crowded environment, which could be of great importance in real biological systems.

ACKNOWLEDGMENTS

This work is supported by National Basic Research Program of China (Grant No. 2013CB834606), by National Science Foundation of China (Grants No. 21673212, No. 21521001, No. 21473165, and No. 21403204), by the Ministry of Science and Technology of China (Grant No. 2016YFA0400904), and by the Fundamental Research Funds for the Central Universities (Grants No. WK2060030018, No. 2030020028, and No. 2340000074).

APPENDIX: REPLICA ORNSTEIN-ZERNIKE EQUATIONS

In this appendix, we briefly outline the replica Ornstein-Zernike (ROZ) equations we used to calculate the static properties of the system. As discussed in the section of model and theory, we need to obtain the structure factors ($S_q^{(ff)c}$, $S_q^{(ff)b}$, S_q^{fm}, S_q^{mm}), direct correlations functions among the tagged particle and the fluid or matrix particles (c_q^{ff}, c_q^{sf}, c_q^{sm}), and the total correlation function $h_q^{ss(b)}$, and so on. The ROZ equations are similar to the usual OZ equations for a two-component fluid system, nevertheless, now the total correlation function h_q^{ff} or direct correlation function c_q^{ff} of the fluid component, which are the Fourier transformation of the total and direct correlation functions $h^{ff}(r)$ and $c^{ff}(r)$, respectively, now contains a connected part and a blocked part. Consequently, the ROZ equations for the fluid-matrix system are given by

$$h_q^{mm} = c_q^{mm} + n_m c_q^{mm} h_q^{mm}, \tag{A1}$$

$$h_q^{fm} = c_q^{fm} + n_m c_q^{fm} h_q^{mm} + n_f c_q^{ff(c)} h_q^{fm}, \tag{A2}$$

$$h_q^{ff(b)} = c_q^{ff(b)} + n_m c_q^{fm} h_q^{fm} + n_f c_q^{ff(c)} h_q^{ff(b)} + n_f c_q^{ff(b)} h_q^{ff(c)}, \tag{A3}$$

$$h_q^{ff(c)} = c_q^{ff(c)} + n_f c_q^{ff(c)} h_q^{ff(c)}, \tag{A4}$$

where $c_q^{ff} = c_q^{ff(c)} + c_q^{ff(b)}$ and $h_q^{ff} = h_q^{ff(c)} + h_q^{ff(b)}$. With these correlation functions, the structure factors can be obtained easily via the following relations [30]:

$$S_q^{mm} = 1 + n_m h_q^{mm}, \tag{A5}$$

$$S_q^{fm} = \sqrt{n_f n_m} h_q^{fm}, \tag{A6}$$

$$S_q^{ff(c)} = 1 + n_f h_q^{ff(c)}, \tag{A7}$$

$$S_q^{ff(b)} = n_f h_q^{ff(b)}. \tag{A8}$$

One can also write down a couple of equations for the single-particle part correlation functions such as c_q^{sf}, h_q^{sm}, etc., as those already presented in the Appendix of Ref. [30]. Nevertheless, in the present paper, we consider that the tagged particle is of the same size as the fluid particle, such that the correlation functions among the tagged-particle and the fluid particle is the same as that among fluid-particles, for instance, $c_q^{sm} = c_q^{fm}$ and $c_q^{sf} = c_q^{ff}$. The total correlation function $h_q^{ss(b)}$ can then be calculated from Eq. (30) in the main text. Therefore, we only need to solve the ROZ Eqs. (A1)–(A4) to get related static properties.

There are a lot of methods to solve the ROZ equations shown above. In the present paper, we just used the picard iteration method [47], which is described briefly below for self-consistency. Note that Eq. (A1) can be solved independently with proper closure, while Eqs. (A2)–(A4) are coupled together. Thus, we can first solve Eq. (A1) with the PY closure. The iteration equations then read

$$\Gamma_{mm}(q) = \frac{n_m C_{mm}^2(q)}{q - n_m C_{mm}(q)}, \tag{A9}$$

$$C_{mm}(r) = f(r)[r + \Gamma_{mm}(r)], \tag{A10}$$

with $C_{mm}(q) = q c_q^{mm}$ and $\Gamma_{mm}(q) = q\gamma_q^{mm}$, where $\gamma_q^{mm} = h_q^{mm} - c_q^{mm}$. $f(r)$ is the mayer function given by $\exp(-\frac{V(r)}{k_B T})$, where $V(r)$ denotes the hard-sphere potential among the matrix particles. By this iteration procedure till convergence, one can get γ_q^{mm} and h_q^{mm} can be easily obtained in combination with Eq. (A1).

To solve Eqs. (A2)–(A4), we need to know the form of $c_q^{ff(b)}$. As mentioned in Ref. [48], $c_{ff}^b(r) = 1 + h_{mm}(r)$ if $r < d$ and $c_{ff}^b(r) = c_{mm}(r)$ if $r \geqslant d$, where d is the diameter of fluid particle. After obtaining h_q^{mm} and $c_{ff}^b(r)$ thus $c_q^{ff(b)}$, we can calculate the other variables by the following set of equations [48] corresponding to Eqs. (A2)–(A4):

$$\Gamma_{fm}(q) = -C_{fm}(q) + \frac{C_{fm}(q)\chi(q)}{q - n_f C_{ff}(q) + n_f C_{ff}^b(q)}, \tag{A11}$$

$$\Gamma_{ff}(q) = -C_{ff}(q) + \frac{q^2 C_{ff}(q) + n_m C_{fm}^2(q)\chi(q) - q n_f \left[C_{ff}^c(q)\right]^2}{\left[q - n_f C_{ff}(q) + n_f C_{ff}^b(q)\right]^2}, \tag{A12}$$

$$\Gamma_{ff}^b(q) = -C_{ff}^b(q) + \frac{q^2 C_{ff}^b(q) + n_m C_{fm}^2(q)\chi(q)}{\left[q - n_f C_{ff}(q) + n_f C_{ff}^b(q)\right]^2}, \tag{A13}$$

where $C_{\alpha\beta}(q) = q c_q^{\alpha\beta}$, $C_{\alpha\beta}^b(q) = q c_q^{\alpha\beta(b)}$, $\Gamma_{\alpha\beta}(q) = q\gamma_q^{\alpha\beta}$, with $\gamma_q^{\alpha\beta} = h_q^{\alpha\beta} - c_q^{\alpha\beta}$ (α, β stands for f or m), and $\chi(q) = q + n_m q h_q^{mm}$. Since $c_q^{ff} = c_q^{ff(b)} + c_q^{ff(c)}$, these equations can solve the three unknown variables c_q^{fm}, $c_q^{ff(b)}$, and $c_q^{ff(c)}$ with the help of the following PY closures:

$$C_{\alpha\beta}(r) = \begin{cases} -r - \Gamma_{\alpha\beta}(r) & r < \sigma_{\alpha\beta} \\ C_{ff}^b(r) & r \geqslant \sigma_{\alpha\beta} \end{cases}, \tag{A14}$$

where $\sigma_{\alpha\beta} = \dfrac{d_\alpha + d_\beta}{2}$.

[1] R. Ellis, Trends Biochem. Sci. **26**, 597 (2001).
[2] A. S. Verkman, Trends Biochem. Sci. **27**, 27 (2002).
[3] D. S. Banks and C. Fradin, Biophys. J. **89**, 2960 (2005).
[4] H. Sanabria, Y. Kubota, and M. N. Waxham, Biophys. J. **92**, 313 (2007).
[5] V. Pryamitsyn and V. Ganesan, Phys. Rev. Lett. **100**, 128302 (2008).
[6] T. Kalwarczyk, N. Ziębacz, A. Bielejewska, E. Zaboklicka, K. Koynov, J. Szymański, A. Wilk, A. Patkowski, J. Gapiński, H.-J. Butt *et al.*, Nano. Lett. **11**, 2157 (2011).
[7] T. Garg, O. Singh, S. Arora, and R. S. R. Murthy, Crit. Rev. Ther. Drug. Carrier Syst. **29**, 1 (2012).
[8] S. Qin, L. Cai, and H.-X. Zhou, Phys. Biol. **9**, 066008 (2012).
[9] H. Matsuda, G. G. Putzel, V. Backman, and I. Szleifer, Biophys. J. **106**, 1801 (2014).
[10] A. J. Ellery, M. J. Simpson, S. W. McCue, and R. E. Baker, J. Chem. Phys. **140**, 054108 (2014).
[11] D. Normanno, L. Boudarène, C. Dugast-Darzacq, J. Chen, C. Richter, F. Proux, O. Bénichou, R. Voituriez, X. Darzacq, and M. Dahan, Nat. Commun. **5**, 4683 (2014).
[12] H. Li, S.-X. Dou, Y.-R. Liu, W. Li, P. Xie, W.-C. Wang, and P.-Y. Wang, J. Am. Chem. Soc. **137**, 436 (2015).
[13] Q. Xiao, M. Gu, H. Yang, B. Li, C. Zhang, Y. Liu, F. Liu, F. Dai, L. Yang, Z. Liu *et al.*, Nat. Commun. **6**, 8844 (2015).
[14] D. Miyoshi and N. Sugimoto, Biochimie **90**, 1040 (2008).
[15] J. A. Dix and A. S. Verkman, Annu. Rev. Biophys. **37**, 247 (2008).
[16] C. Echeverria and R. Kapral, Phys. Chem. Chem. Phys. **14**, 6755 (2012).
[17] C. Echeverria and R. Kapral, Phys. Chem. Chem. Phys. **17**, 29243 (2015).
[18] L. Stagg, S.-Q. Zhang, M. S. Cheung, and P. Wittung-Stafshede, Proc. Natl. Acad. Sci. U.S.A. **104**, 18976 (2007).
[19] C. D. Rienzo, V. Piazza, E. Gratton, F. Beltram, and F. Cardarelli, Nat. Commun. **5**, 5891 (2014).
[20] M. C. Konopka, I. A. Shkel, S. Cayley, M. T. Record, and J. C. Weisshaar, J. Bacteriol. **188**, 6115 (2006).
[21] T. Ando and J. Skolnick, Proc. Natl. Acad. Sci. U.S.A. **107**, 18457 (2010).
[22] B. P. Bratton, R. A. Mooney, and J. C. Weisshaar, J. Bacteriol **193**, 5138 (2011).
[23] T. Pederson, Nat. Cell Biol. **2**, E73 (2000).
[24] H. Fukuoka, T. Sagawa, Y. Inoue, H. Takahashi, and A. Ishijima, Sci. Signal **7**, ra32 (2014).
[25] M. Patrick, P. P. Dennis, M. Ehrenberg, and H. Bremer, Biochimie **119**, 80 (2015).
[26] P. L. Luisi, M. Allegretti, T. P. de Souza, F. Steiniger, A. Fahr, and P. Stano, ChemBioChem **11**, 1989 (2010).
[27] A. P. Minton, J. Biol. Chem. **276**, 10577 (2001).
[28] V. Krakoviack, Phys. Rev. Lett. **94**, 065703 (2005).
[29] V. Krakoviack, Phys. Rev. E **75**, 031503 (2007).
[30] V. Krakoviack, Phys. Rev. E **79**, 061501 (2009).
[31] M. Doi and S. F. Edwards, *The Theory of Polymer Dynamics* (Oxford University Press, Oxford, 1986).
[32] P. G. de Gennes, J. Chem. Phys. **55**, 572 (1971).
[33] W. J. Briels, *Theory of Polymer Dynamics* (Oxford University Press, Oxford, 1998).
[34] J. Tang and R. A. Marcus, Phys. Rev. E **73**, 022102 (2006).
[35] P. Li, Y. Dong, N. Zhao, and Z. Hou, J. Chem. Phys. **140**, 154109 (2014).
[36] S. Bhattacharyya and B. Bagchi, J. Chem. Phys. **106**, 7262 (1997).
[37] Y. Dong, X. Feng, N. Zhao, and Z. Hou, J. Chem. Phys. **143**, 024903 (2015).
[38] U. Yamamoto and K. S. Schweizer, Macromolecules **48**, 152 (2014).

[39] S. Bhattacharyya and B. Bagchi, J. Chem. Phys. **106**, 1757 (1997).
[40] S. M. Ali, A. Samanta, and S. K. Ghosh, J. Chem. Phys. **114**, 10419 (2001).
[41] S. A. Egorov, J. Chem. Phys. **134**, 084903 (2011).
[42] I. Goychuk, Phys. Rev. E **80**, 046125 (2009).
[43] A. J. Moreno and J. Colmenero, Phys. Rev. Lett. **100**, 126001 (2008).
[44] B. J. Sung and A. Yethiraj, J. Chem. Phys. **123**, 074909 (2005).
[45] R. Chang and A. Yethiraj, J. Chem. Phys. **126**, 174906 (2007).
[46] B. J. Sung, R. Chang, and A. Yethiraj, J. Chem. Phys. **130**, 124908 (2009).
[47] H. H. H. Homeier, S. Rast, and H. Krienke, Comput. Phys. Commun. **92**, 188 (1995).
[48] E. Lomba, J. A. Given, G. Stell, J. J. Weis, and D. Levesque, Phys. Rev. E **48**, 233 (1993).